Efficient *A Posteriori* Error Estimation for Finite Volume Methods

Richard P. Dwight

Institute of Aerodynamics and Flow Technology
German Aerospace Center (DLR)
Braunschweig, D-38108
GERMANY

Tel: +49 531 295 2893

Email: richard.dwight@dlr.de

ABSTRACT

The propagation of error in numerical solutions of the compressible Navier-Stokes equations is examined using linearized, and adjoint linearized versions of the discrete flow solver. With the forward linearization it is possible, given a measure of the local residual error in the field, to obtain estimates of global solution error. This allows for example the computation of error estimates on pressure distributions. With the backward or adjoint linearization it is possible, for any given scalar output quantity, to identify those regions of the field which contribute the most to the error in that quantity. This information may be used to refine the mesh in a way that minimizes error in this output functional. Both approaches are be used, not only to provide accurate error estimates, but also to correct the output. In the following we concentrate on the solution error due to explicitly added artificial dissipation in the spatial discretization. By comparing with the true solution error obtained using mesh refinement studies, it is seen that this can be applied as an effective total error indicator for mesh adaptation.

1.0   INTRODUCTION

There are many situations in numerical simulation where some measure of residual error is known or cheaply available, but the solution error is desired. A common example is in a partially converged stationary simulation, where the magnitude of the spatial residual is used as a convergence indicator, but provides no explicit information about the level of error in the solution caused by the lack of full convergence. Another example is the residual error between the spatial discretization and the continuous equation, which may be estimated relatively cheaply, but which again say little about solution accuracy. In order to convert residual error into a leading-order approximation of solution error, a linear system may be solved as follows.

Consider a stationary non-linear problem $R_h(w) = 0$, w being flow variables and R_h a spatial discretization operator, also incorporating boundary conditions. Then if $\tilde{R}$ is some measure of residual error,

$$\frac{\partial R}{\partial w} \Delta w = \tilde{R},$$

may be solved for Δw, a corresponding solution error estimate.

In essence it is this simple procedure, and it's effectiveness in estimating discretization error when applied to the compressible Navier-Stokes equations — where the residual error is taken to be explicitly added artificial dissipation in the numerical scheme — that will be examined in this paper.

Apart from the choice of residual there are several issues and extensions to the basic idea that must be discussed. Firstly, by considering the adjoint equation, rather than the linearized equation above, it is possible to quantify the influence regions in the computational domain have on the error in a specified scalar quantity of interest, denoted J. This information allows meshes to be locally adapted in such a way that error in J is minimized. Secondly the construction and solution of the linear system above (and its adjoint equivalent) for complex flow solvers with a wide range of boundary conditions and turbulence models is a delicate problem, which has only recently become possible for large three-dimensional test cases. Finally the effectiveness of the technique in practical problems is addressed, in particular how well-resolved the solution must be before the error estimator (which assumes the error may be regarded as a linear perturbation) is effective.

After a description of the theory, implementation details are discussed, before the method is applied to error estimation for 2d viscous flows, and error estimation and adaptation for 2d and 3d inviscid flows. The solver used throughout is an unstructured finite volume compressible Navier-Stokes solver, the DLR TAU-Code [1, 2].

2.0 COMPRESSIBLE VISCOUS FINITE VOLUME FLOW SOLVER

The unstructured grid, finite volume, compressible Favre-averaged Navier-Stokes solver, the DLR *TAU*-Code, is briefly described in order to provide context for the subsequent error estimator and numerical results (more detailed presentations may be found in [1] and [2]). The code will also be used in inviscid mode by removing viscous terms, turbulence model, and setting slip boundary conditions.

2.1 Navier-Stokes Equations

The compressible Favre averaged Navier-Stokes equations with adiabatic boundary conditions may be written in conservative variables $w = (\rho, \rho u_x, \rho u_y, \rho E)$, and in two dimensions on a domain Ω with boundary Γ, itself with normal vector n_Γ as

$$\frac{\partial w}{\partial t} + \nabla \cdot (f^c(w) - f^v(w)) = 0 \quad \text{in} \quad \Omega,$$

$$u = 0, \quad \nabla T \cdot n_\Gamma = 0 \quad \text{on} \quad \Gamma,$$

whereby we will later refer to the complete spatial term in the above equation as the *continuous residual* $\mathcal{R}(w)$, so that the stationary flow problem may be formulated as $\mathcal{R}(w) = 0$. Here ρ is the fluid density, E the total energy, and $u = (u_x, u_y)$ the Cartesian velocity components. The convective and viscous fluxes tensors in the direction of an arbitrary normal vector n are respectively

$$f^c \cdot n = \begin{bmatrix} \rho V \\ \rho u_x V + p n_x \\ \rho u_y V + p n_y \\ \rho H V \end{bmatrix}, \quad f^v \cdot n = \begin{bmatrix} 0 \\ \tau_{xi} n_i \\ \tau_{yi} n_i \\ \tau_{zi} n_i \\ \tau_{ij} n_i u_j + \kappa \nabla_i T n_i \end{bmatrix},$$

where $V = u_i n_i$, and the summation convention is used above. The fluid temperature is defined over $T = p/(\rho \Re)$ where $\Re$ is the universal gas constant, and κ is the local thermal conductivity. The pressure p is

specified for a calorically perfect gas with ratio of specific heats γ, by the state equation

$$p = (\gamma - 1)\rho \left\{ E - \frac{1}{2} u \cdot u \right\}.$$

The viscous shear stress tensor τ is given by

$$\tau = \mu \left(\nabla u + \nabla u^T \right) + \lambda \nabla \cdot u I,$$

where I is the identity matrix. To obtain the bulk viscosity λ from the molecular viscosity μ we employ Stokes hypothesis for a monatomic gas: $\lambda = -(2/3)\mu$. By making the Boussinesq eddy viscosity assumption the influence of turbulence on the averaged equations above may be accounted for by modifying μ and with some eddy viscosity μ_t provided by a turbulence transport model. In the following we apply the one-equation model of Spalart and Allmaras with Edwards modification (SAE) [3].

2.2 Finite Volume Discretization

Consider the governing equations specified on a finite set of closed control volumes $\Omega_i \subset \Omega$ which cover the domain Ω completely and intersect with each other only on their boundaries Γ_i, thereby forming a computational mesh $\mathcal{M}_h = \{\Omega_i : \forall i\}$. Continuous functions are approximated on this mesh as members of the space

$$\mathcal{V}_{h,p} := \{v : v \in \mathcal{P}_p(\Omega_i), \forall i\},$$

where $\mathcal{P}_p(\Omega)$ is the space of polynomials of degree $\leq p$ restricted to the volume Ω. Note that $\mathcal{V}_h$ is in general discontinuous and multivalued on the boundary of two neighbouring control volumes $\Gamma_{ij} := \Omega_i \cap \Omega_j$. For each control volume we have

$$\int_{\Omega_i} \nabla \cdot (f^c - f^v) \, d\Omega = \int_{\Gamma_i \backslash \Gamma} (f^c - f^v) \cdot n \, d\Gamma + \int_{\Gamma_i \cap \Gamma} (f^c - f^v) \cdot n|_{u=0, \nabla T \cdot n=0} \, d\Gamma,$$

but since $w \in \mathcal{V}_h$, f^c and f^v are multivalued on Γ_{ij} and must be replaced with numerical fluxes across control volume faces $\hat{f}^c(w; n)$ and $\hat{f}^v(w; n)$. It is well known that $\hat{f}^c$ must contain some added dissipation if the discretization is to be numerically stable. This may be achieved by upwinding, or explicit addition of artificial viscosity.

One common approach used to obtain a second order accurate method is to take $p = 1$ and let $\hat{f}^c$ be an upwind flux such as Roe. Here however we concentrate on $p = 0$ thereby requiring only one degree of freedom per flow quantity per control volume, and no solution reconstruction operator. Second order is achieved by use of the Jameson-Schmidt-Turkel (JST) flux [4] which consists of a central difference of the convective flux plus first and third order artificial dissipation terms, with a shock switch to weight the two. For a mesh face Γ_{ij} with normal n_{ij} the flux is

$$\hat{f}^c(w; n_{ij}) := \frac{1}{2} \left(f^c(w_i) + f^c(w_j) \right) \cdot n_{ij} - \frac{1}{2} |\lambda_{ij}| \left[\varepsilon_{ij}^{(2)} \{w_j - w_i\} - \varepsilon_{ij}^{(4)} \{L_j(w) - L_i(w)\} \right], \qquad (1)$$

where w_i are the conservative variables in Ω_i, $|\lambda_{ij}|$ is the maximum convective eigenvalue at the face, and

$$\varepsilon_{ij}^{(2)} := k^{(2)} \max(\Psi_i, \Psi_j) \Phi^{(2)}, \quad \varepsilon_{ij}^{(4)} := \max(k^{(4)} - \varepsilon_{ij}^{(2)}, 0) \Phi^{(4)},$$

$$L_i(w) := \sum_{j \in \mathcal{N}(i)} (w_j - w_i), \quad \Psi_i := \frac{\sum_{j \in \mathcal{N}(i)} (p_j - p_i)}{\sum_{j \in \mathcal{N}(i)} (p_j + p_i)},$$

where $\mathcal{N}(i)$ is the set of control volume neighbours of i, Ψ is the shock switch, which is large when the gradient of pressure p is large, and thereby serves to identify discontinuities. The Φ contain some heuristic mesh anisotropy corrections which aid absolute accuracy on irregular unstructured meshes. Finally $k^{(2)}$, $k^{(4)}$ are constants, by default $\frac{1}{2}$ and $\frac{1}{64}$ respectively, through which the absolute level of 2nd- and 4th-order dissipation, and hence the compromise between stability and accuracy may be adjusted. However for the purposes of the estimation of error due to dissipation in the following we will also regard them as variable.

The shock switch Ψ is designed to be $\mathcal{O}(1)$ near regions of large pressure gradient and $\mathcal{O}(h^2)$ elsewhere, where h is the characteristic mesh spacing. Hence near a shock $\varepsilon^{(2)} \sim \mathcal{O}(1)$ and $\varepsilon^{(4)} = 0$, so that the scheme does not attempt to construct a fourth-derivative using a stencil which crosses a discontinuity. In smooth regions $\varepsilon^{(2)} \sim \mathcal{O}(h^2)$ and $\varepsilon^{(4)} \sim \mathcal{O}(1)$, so that both second- and fourth-differences are active and of $\mathcal{O}(h^3)$. Away from shocks the scheme is therefore second-order accurate in h as a result of the central difference in (1).

Discretization of the viscous terms tends to be much less critical; solution gradients are approximated using a Green-Gauss formula,

$$\nabla w_i \simeq g_i(w) := \frac{1}{\|\Omega_i\|} \sum_{j \in \mathcal{N}(i)} \frac{1}{2}(w_i + w_j)n_{ij},$$

and a central average of the viscous flux f^v on each side of the face is taken, $\hat{f}^v(w; n_{ij}) := \frac{1}{2}(f^v(w_i, g_i(w)) + f^v(w_j, g_j(w))) \cdot n_{ij}$. The SAE turbulence transport equation is discretized in a similar way to the mean-flow equations, with the exception that a first order accurate scalar upwind scheme is used for the convective terms.

In the following the complete spatial discretization on mesh $\mathcal{M}_h$ incorporating all terms and boundary conditions is denoted R_h, so that the discrete problem may be written simply $R_h(w_h) = 0$.

3.0 *A POSTERIORI* ERROR ESTIMATION

The work on error estimation discussed in the introduction, with the exception of that of Cavallo [5], has been almost exclusively performed in terms of an adjoint formulation for the error in a single scalar functional of interest $\mathcal{J}$. This has the advantage of quantifying the influence of local error production at all points of the domain on error in $\mathcal{J}$, providing in addition to an *estimate* of the error in $\mathcal{J}$ a means of reducing that error via an *indicator* for mesh adaptation. However by considering instead the direct (*primal*) linearization, in the following an *a posteriori* error estimate for *all* output quantities may be computed simultaneously with the solution of a single linearized flow problem with suitable source terms, an *error transport equation* (ETE) [5].

The derivation of error estimators for general non-linear operators $\mathcal{R}$ is complicated by necessity of introducing the *mean value linearization* in order to relate a difference of residuals $\mathcal{R}(w) - \mathcal{R}(w_h)$ to a difference of solutions $(w - w_h)$. This device tends to cloud more critical aspects of the derivation, so in Section 3.1 the theory will be presented first for a linear operator $\mathcal{L}$ and linear functional of interest g, for which the estimator is also exact. The non-linear generalization is given in Section 3.2, and necessary approximations in order to obtain an estimator which may be readily computed are discussed in Section 3.3. The implementation of the linear and adjoint versions of the flow solver is described in Section 3.4.

3.1 Error Representation for Linear Problems

Consider the linear problem

$$\mathcal{L}u = f, \tag{2}$$

with unknown vector u and known right-hand side f. Let the functional of interest be of the form $J = (g, u)$, where the inner product over the problem domain $(\cdot, \cdot)$ is defined by $(u, v) = \int_\Omega u \cdot v \, d\Omega$, and define the

corresponding adjoint (or dual) problem

$$\mathcal{L}^* v = g, \tag{3}$$

whose solution v satisfies the dual equivalence relation

$$(g, u) = (\mathcal{L}^* v, u) = (v, \mathcal{L} u) = (v, f), \tag{4}$$

by definition of $\mathcal{L}^*$. Now let $u_h \in \mathcal{V}_h$ be the exact discrete solution of some discretization of (2), $L_h u_h = f_h$ where the subscript h indicates discretization. The extent to which the approximate solution u_h does not satisfy the continuous governing equation may be written as the residual $r_h := f - \mathcal{L} u_h$. The error in u_h may be written $\epsilon_h := (u - u_h)$ which clearly satisfies

$$\mathcal{L} \epsilon_h = r_h, \tag{5}$$

by linearity. Given ϵ_h the error in any functional $J(u) - J(u_h)$ may be directly evaluated as an inner product: $J(u) - J(u_h) = (g, \epsilon_h)$.

The error in J may equally be evaluated with reference to the dual problem as follows:

$$
\begin{aligned}
J(u) - J(u_h) &= (g, u) - (g, u_h) \\
&= (g, u - u_h) \\
&= (\mathcal{L}^* v, u - u_h) \\
&= (v, \mathcal{L}(u - u_h)) \\
&= (v, f - \mathcal{L} u_h) \\
&= (v, r_h),
\end{aligned}
$$

where one adjoint problem (equivalent in effort to the original linear problem) must be solved for each (scalar) functional of interest J. The importance of this dual formulation of the error is that it quantifies the influence local residual error in the domain on error in J.

This may be seen by noting that the adjoint solution v may be generally interpreted as quantifying the influence of a point source of mass, momentum or energy at each point in the domain on J [6]. Where this influence and the residual r_h are simultaneously large, a large contribution is made to the inner product (v, r_h) and hence the error in J. Where either the residual is small, or where the point in question has little influence, a small contribution is made. Hence the error in J has been expressed as a sum of contributions from each point in the domain, and may be most effectively reduced by reducing r_h where the contributions are greatest. The reduction in r_h is typically achieved using local mesh refinement.

Note that if one is interested in minimizing error by mesh adaptation in n distinct functionals J_i, for example the six forces and moments on a three-dimensional body, then one must solve n adjoint problems (albeit with the same operator $\mathcal{L}^*$, and hence the same system matrix). A method for reducing this effort to one forward and one adjoint problem for arbitrary n is alluded to in Section 5.0 in the context of future work.

Returning to the error estimators, in summary

$$J(u) - J(u_h) = (g, \epsilon_h) = (v, r_h),$$

which may be compared with the primal-dual equivalence relation (4). Note that both primal and dual formulations require the solution of a single linear system in $\mathcal{L}$.

3.2 Error Representation for Non-linear Problems

Now consider the non-linear problem

$$\mathcal{R}(w) = 0, \tag{6}$$

with non-linear functional of interest $\mathcal{J}(w)$. Assume there exist Fréchet derivatives of $\mathcal{R}$ and $\mathcal{J}$, $\mathcal{R}'[w]\tilde{w}$ and $(\mathcal{J}'[w], \tilde{w})$ respectively, $\forall \tilde{w}$. Define the *mean value linearization* (MVL) $\bar{\mathcal{R}}'[w, w_h]$ of $\mathcal{R}$ between the solution of (6) and some discrete solution w_h as

$$\bar{\mathcal{R}}'[w, w_h] = \int_0^1 \mathcal{R}'[w + \theta(w_h - w)]\,\mathrm{d}\theta,$$

so that

$$\mathcal{R}(w_h) - \mathcal{R}(w) = \int_0^1 \frac{\partial}{\partial\theta}\mathcal{R}(w + \theta(w_h - w))\,\mathrm{d}\theta = \bar{\mathcal{R}}'[w, w_h](w_h - w), \tag{7}$$

whereby the first equality follows from the fundamental theorem of calculus, and the second from the chain rule. Note that this device depends upon the existence of Fréchet derivatives of $\mathcal{R}$ for a continuum of solutions between w_h and w. Similarly for $\mathcal{J}$ let

$$\bar{\mathcal{J}}'[w, w_h] = \int_0^1 \mathcal{J}'[w + \theta(w_h - w)]\,\mathrm{d}\theta, \quad \text{so that} \quad \mathcal{J}(w_h) - \mathcal{J}(w) = (\bar{\mathcal{J}}'[w, w_h], w_h - w).$$

As before we may also define the dual problem:

$$\mathcal{R}'^*[w_h]\psi_h = \mathcal{J}'[w_h], \tag{8}$$

with adjoint variable ψ_h and corresponding equivalence relation

$$(\mathcal{J}'[w_h], \tilde{w}) = (\mathcal{R}'^*[w_h]\psi_h, \tilde{w}) = (\psi_h, \mathcal{R}'[w_h]\tilde{w}). \tag{9}$$

From (7) an expression for the solution error $\epsilon_h := w - w_h$ is directly obtained

$$\bar{\mathcal{R}}'[w, w_h]\epsilon_h = \mathcal{R}(w_h), \tag{10}$$

corresponding to (5). One important difference to the linear case is that (10) contains the exact solution of the continuous problem within the MVL. To remove this dependence we approximate $\bar{\mathcal{R}}'[w, w_h]$ by $\mathcal{R}'[w_h]$, which may be shown to result in an $\mathcal{O}\|w_h - w\|^2$ modification to ϵ_h. Given ϵ_h, the error in functionals may be estimated as $(\bar{\mathcal{J}}'[w, w_h], \epsilon_h) \simeq (\mathcal{J}'[w_h], \epsilon_h) + \mathcal{O}\|w_h - w\|^2$, but also directly as $\mathcal{J}(w_h) - \mathcal{J}(w_h + \epsilon_h)$.

If the only error of interest is that in $\mathcal{J}$ then the adjoint problem may be used to obtain an alternative expression for the error:

$$
\begin{aligned}
\mathcal{J}(w_h) - \mathcal{J}(w) &= (\bar{\mathcal{J}}'[w, w_h], w_h - w) \\
&\simeq (\mathcal{J}'[w_h], w_h - w) \\
&= (\mathcal{R}'^*[w_h]\psi_h, w_h - w) \\
&= (\psi_h, \mathcal{R}'[w_h](w_h - w)) \\
&\simeq (\psi_h, \bar{\mathcal{R}}'[w, w_h](w_h - w)) \\
&= (\psi_h, \mathcal{R}(w_h)),
\end{aligned}
\tag{11}
$$

where the final equality uses $\mathcal{R}(w) = 0$, and the terms neglected in the approximate equalities above are of the order of $\|w_h - w\|^2$ and $\|w_h - w\|\|\psi_h - \psi\|$, where ψ is the solution of the adjoint problem $\mathcal{R}'^*[w]\psi = \mathcal{J}'[w]$. Thus the error in $\mathcal{J}$ is recast in terms of solutions of the discrete problem and its adjoint, without reference to the solution of the original continuous problem. As in the linear case the integrand of $(\psi_h, \mathcal{R}(w_h))$ may be used to locate contributions to error in $\mathcal{J}$, and reduce it via local mesh refinement.

In summary for the non-linear case, again in reference to the primal-dual equivalence relation (9), we have the following approximate expressions for the functional error:

$$\mathcal{J}(w) - \mathcal{J}(w_h) \simeq (\mathcal{J}'[w_h], \epsilon_h) \simeq (\psi_h, \mathcal{R}(w_h)), \tag{12}$$

with no dependence on the exact solution w.

3.3 Computable Error Estimates and Adaptation Indicators

In the remainder of this work only the non-linear case is considered. The expressions for error given in (12) are not useful in practice, as they rely on solutions of the (continuous) linearized governing equations, either in the adjoint (8) or forward (10) form. These are replaced with discretizations of the linearized equations; in our work on the same mesh on which the flow solution is computed, and with the linearization of the non-linear discretization. Unlike the Galerkin case it is not necessary to obtain an adjoint solution of higher accuracy than original flow problem, however doing so, either with a higher-order method or on a globally refined mesh, will tend to improve the accuracy of the error estimate [7]. However, such approaches will always remain many times more computationally expensive than the flow problem itself, and as such are likely only ever to be of limited use in an engineering context.

It remains to approximate the continuous residual of the discrete solution: $\mathcal{R}(w_h)$ (obviously using the existing discrete residual R_h is not acceptable, as $R_h(w_h) = 0$). Two approaches are: to evaluate the residual, (a) with a higher-order version of the same method [8–12], or (b) on a globally refined mesh [13–16]. A higher-order version of the solver we are currently using is not readily available, and there are substantial difficulties associated with approach (b). In particular second-order interpolation of discontinuous solutions from coarse grids onto fine grids is needed. Also efficient evaluation of the fine grid residual without explicit construction and storage of this grid is difficult; explicit storage would represent a memory bottleneck.

Instead we pursue an idea already explored in [17, 18] of taking the level of explicitly added artificial dissipation as a measure of the local residual error. The artificial dissipation may be interpreted as an unphysical term which modifies the governing equations, and hence as an error. An empirical analysis of the proportion of total discretization error due to the explicitly added dissipation for the DLR *Tau*-code has been conducted, and is described in [18]. It has already been noted that the dissipation terms for smooth solutions vary at third-order in the mesh spacing h, while the central discretization of the fluxes is second-order accurate. Hence for sufficiently fine meshes the latter will eventually dominate and an error estimator based on dissipation will be ineffective. Hence the study already mentioned was conducted at a variety of mesh resolutions, and it was seen that even for slowly varying flows on extremely fine meshes (a subsonic NACA0012 aerofoil in 2d with 1×10^5 grid points), more than 90% of the discretization error could be ascribed to the dissipation terms. Therefore neglecting other sources of discretization error may be justified.

Such an analysis immediately suggests (assuming perturbations to the solution are sufficiently small for first-order effects to dominate) an *a posteriori* error estimator for dissipation in the JST scheme:

$$\eta = k^{(2)} \frac{\mathrm{d}J}{\mathrm{d}k^{(2)}} + k^{(4)} \frac{\mathrm{d}J}{\mathrm{d}k^{(4)}}. \tag{13}$$

This construction is closely related to the estimators already discussed, as may be seen if we consider evaluating the derivatives above using the adjoint as follows. Consider the Lagrangian: $\mathcal{L}(w, \psi) = J(w) + \psi^T R(w)$, which always takes the value J provided the state equation $R(w) = 0$ is fulfilled. Then also $\mathrm{d}J/\mathrm{d}k = \mathrm{d}\mathcal{L}/\mathrm{d}k$, so that

$$\frac{\mathrm{d}J}{\mathrm{d}k} = \frac{\mathrm{d}\mathcal{L}}{\mathrm{d}k} = \frac{\partial J}{\partial w}\frac{\mathrm{d}w}{\mathrm{d}k} + \psi^T \left\{ \frac{\partial R}{\partial k} + \frac{\partial R}{\partial w}\frac{\mathrm{d}w}{\mathrm{d}k} \right\} \tag{14}$$

$$= \left\{ \frac{\partial J}{\partial w} + \psi^T \frac{\partial R}{\partial w} \right\} \frac{\mathrm{d}w}{\mathrm{d}k} + \psi^T \frac{\partial R}{\partial k} = \psi^T \frac{\partial R}{\partial k}, \tag{15}$$

whereby the final equality holds if ψ satisfies the adjoint equation

$$\frac{\partial R}{\partial w}^T \psi = -\frac{\partial J}{\partial w}^T .$$

Substituting (15) into (13) gives

$$\eta = \psi \left(k^{(2)} \frac{\partial R}{\partial k^{(2)}} + k^{(4)} \frac{\partial R}{\partial k^{(4)}} \right),$$

which may be seen to be of the same form as (11) with $\mathcal{R}(w_h)$ replaced by a measure of the local dissipation. So the dissipation error estimator may be constructed by two distinct arguments.

The same approach to the derivation may be extended to a dissipation error indicator for J, by considering the influence of *local* variation of dissipation level. Let the dissipation coefficients be interpreted as being defined independently for each control volume,

$$\mathcal{K} = \left\{ k_i^{(2)}, k_i^{(4)} : \forall i \right\}.$$

with the coefficient on a face being an average of immediate neighbours,

$$k_{ij}^{(2)} = \frac{1}{2} \left(k_i^{(2)} + k_j^{(2)} \right), \qquad k_{ij}^{(4)} = \frac{1}{2} \left(k_i^{(4)} + k_j^{(4)} \right).$$

Now $\mathrm{d}J/\mathrm{d}k_i^{(2)}$ for example is a measure of the influence of the second-order dissipation in cell i on J, so an indicator for dissipation-error in J is

$$\xi_i = k^{(2)} \frac{\mathrm{d}J}{\mathrm{d}k_i^{(2)}} + k^{(4)} \frac{\mathrm{d}J}{\mathrm{d}k_i^{(4)}}. \tag{16}$$

Given ψ the only additional computation expense in calculating ν and ξ_i is the evaluation of $\partial R/\partial k$, which may be written down immediately. For $k_j^{(4)}$ for example it is

$$\frac{\partial R_i}{\partial k_j^{(4)}} = \begin{cases} \sum_{m \in \mathcal{N}(i)} -\frac{1}{4} |\lambda_{im}| \{ L_m(w) - L_i(w) \} & j = i \\ -\frac{1}{4} |\lambda_{ij}| \{ L_j(w) - L_i(w) \} & j \in \mathcal{N}(i) \\ 0 & \text{otherwise} \end{cases}, \tag{17}$$

and is always of the same order in mesh spacing h as the original dissipation term, so that away from singularities in the adjoint solution (which occur at sharp trailing edges in 2d transonic flows) the error indicator approaches zero as the mesh is refined.

Note that the relations

$$\sum_i \frac{\partial R_i}{\partial k_j^{(4)}} = 0, \quad \sum_j \frac{\partial R_i}{\partial k_j^{(4)}} = \frac{\partial R_i}{\partial k^{(4)}},$$

hold, so that in particular

$$\eta = \sum_i \xi_i, \tag{18}$$

and the sum of all local error indicators is the total error estimator as expected.

When constructing an approximation for $\mathcal{R}(w_h)$ in the error transport equation on the other hand, the artificial dissipation terms are constructed directly.

3.4   Implementation of Linearized Solvers

The implementation of a solver for the linearized and adjointed governing equations is a non-trivial task requiring considerable effort, and has been investigated intensively in the context of control theory and optimization [19–22]. There are two possible approaches: the *continuous* approach of discretizing the linearized (and subsequently adjointed) continuous equations, exemplified by the work of Jameson and co-authors [20, 23, 24], and the *discrete* approach of linearizing the existing discretization of the non-linear equation [25–27]. The former is limited in the J for which it may be constructed, which causes for example problems with functionals containing skin friction forces [23]. The handling of turbulence models is also problematic in a continuous framework, and has not yet been seen in the literature.

A continuous linearized inviscid solver has recently been used in an error estimation context by Cavallo and Sinha [5]. Here we follow the increasingly popular discrete approach, in which there are two principle difficulties in implementation: (a) the exact construction of the Jacobian $\partial R_h / \partial w$ and (b) the solution of the resulting linear system.

Typically it is the case that R_h may be written explicitly in terms of w, and hence the partial derivative with respect to w may be calculated per hand straightforwardly; while at the same time R_h is extremely complex, containing non-linear fluxes, gradient calculations, limiters, state equations, boundary conditions, turbulence models, etc., etc., and thus the differentiation is extremely tedious, time-consuming and error-prone. Nevertheless this operation must only be performed once. This has been done for our solver, and the result verified against finite differences applied to the original flux routines, see [2]. In order to avoid storing the complete Jacobian, and the resulting impractically high memory costs, methods have also been developed to reduce the storage needed while keeping the cost of matrix-vector product evaluations low, at the cost of some approximations in the Jacobian which have been shown to have negligible influence on results. The method and implementation is discussed in some detail along with parallelization issues in [28]. An analysis of the influence of the approximations was performed in an aerodynamic optimization context in [29].

The solution of the linear system is equally problematic. Stiffness in the non-linear problem (due to high Reynolds numbers, and turbulence models in our problems) is inherited by the linearized equations, and the size of the systems is such that application of standard sparse matrix preconditioners such as ILU factorization rapidly becomes extremely expensive, as well as ineffective in three-dimensions. One solution is to apply existing, well tested iterative techniques for the non-linear equations, either directly (for the error transport equation), or in adjointed form (for the adjoint equation), whereby it may be proven that then the rate of convergence of the linear problems is identical to the asymptotic rate of convergence of the non-linear problem [30, 28]. In our case these iterations are applied as a preconditioner to a restarted GMRES algorithm [31] to increase the robustness of the scheme in cases for which the non-linear iteration does not converge asymptotically [32, 28].

4.0   NUMERICAL RESULTS

The methods described above have been applied to some simple flows about aerofoils and wings, where functionals of interest are taken to be lift coefficient C_L (non-dimensionalized force normal to the onflow direction), and drag C_D (tangent to the onflow direction). Error in non-dimensionalized surface pressure C_P is also examined using the error transport equation.

   The mesh adaptation tool available to us, which takes an original mesh, an adaptation indicator and produces a locally refined mesh, is currently restricted to the refinement of simplices. For viscous flows the solver requires anisotropic rectangular cells for accurate resolution of the boundary-layer, hence goal-oriented adaptation of viscous problems will not be examined here, only the estimation of error in Section 4.1. Adaptation will be applied to two- and three-dimensional inviscid flows in Section 4.2.

   In order to judge the accuracy of the error estimator, an accurate and independent estimate of the true solution error is needed. In the following this is always provided by mesh convergence studies on a sequence of uniformly refined meshes. Where points are added on the surface of the geometry by the refinement, their position is reconstructed using cubic splines. A flow computation is performed on each of these meshes, and Richardson extrapolation on average mesh spacing is applied to C_L and C_D on the three finest results to estimate their limiting value. Where error in C_P distribution is needed, it is estimated as the difference in C_P between the current and finest mesh, as applying Richardson extrapolation to C_P has been seen to give highly oscillatory results.

4.1   Application of the Error Transport Equation

To demonstrate the error transport equation we consider in two-dimensions the RAE 2822 aerofoil at subsonic conditions corresponding to RAE Case 1 of Cook et al. [33], in particular the Mach number is 0.5, and the Reynolds number is taken as 6.5×10^6 with reference to the chord length. Turbulence is modeled with SAE as already mentioned [3], and this model is used in linearized form in the transport equation. The flow is computed on a sequence of five structured meshes, a plot of the coarsest mesh and all C_P distributions are shown in Figure 1. The coarsest mesh (Grid 5) is exceptionally coarse with about 500 cells; each subsequent mesh has four times as many cells. One useful measure of mesh quality for high-Reynolds number flows is the Reynolds number based on height of the first cell at the wall, denoted y^+, which (as a rule of thumb) should be less than one if the boundary-layer is to be well resolved. The finest mesh (Grid 1) with $\approx 130 \times 10^3$ cells has an average y^+ of one, which approximately doubles with each coarser mesh. Hence all but the finest mesh should be considered relatively poor.

   Nonetheless C_L and C_D converge cleanly, see the reference results in Figure 2, allowing confidence to be placed in the Richardson extrapolated values. Estimates of error in the force coefficients obtained from the error transport equation are also plotted, and it may be seen that the agreement between the estimate and the true error is excellent, and tends to improve as the meshes become finer. As well as providing information on the error, the estimates may be used to correct the solution values, and the remaining error in these corrected values is also plotted in Figure 2. In all cases the accuracy of the coefficients is improved, on average by half an order of magnitude.

   Unlike error estimation using the dual approach, errors in C_L and C_D for each mesh above were obtained with a single linear calculation, which provides information regarding error at all points in the domain. The estimated error in C_P from these calculations is plotted in Figure 3, along with difference in C_P between the actual mesh and the finest mesh. Again the two are in good agreement, with the agreement improving as the meshes are refined. Remarkable and satisfying is that the estimator already produces very useful results on
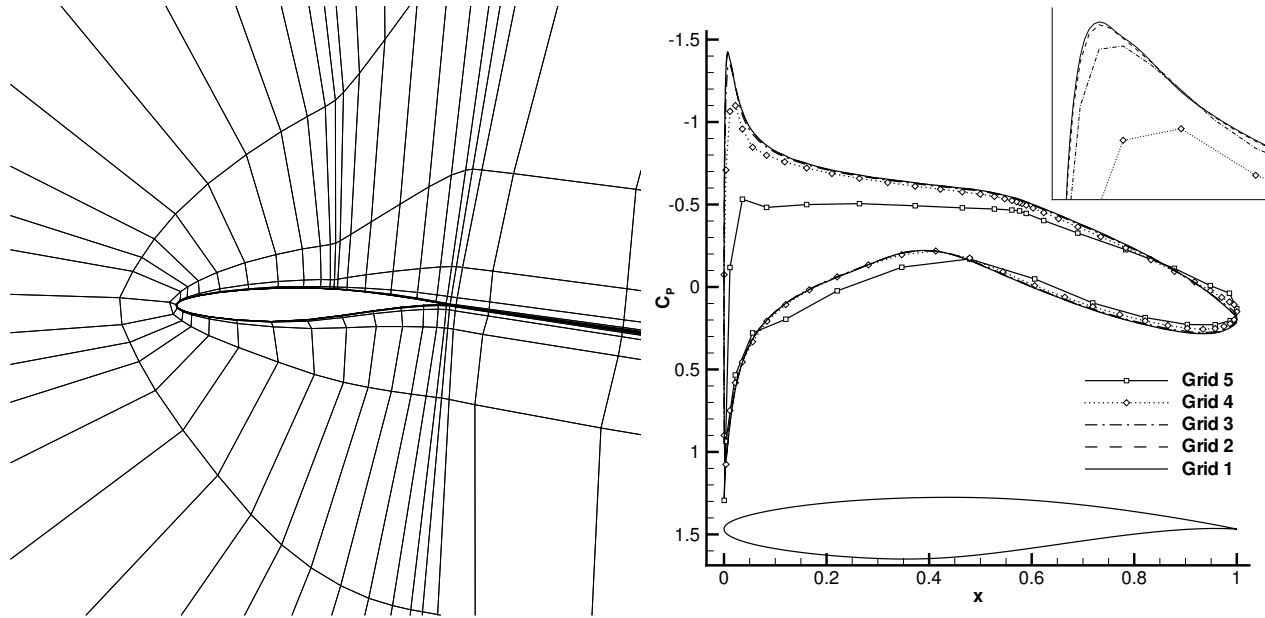
Figure 1: Subsonic turbulent RAE-2822 test-case. Coarsest (Grid 5) mesh (left), pressure coefficient distribution on aerofoil surface (right).
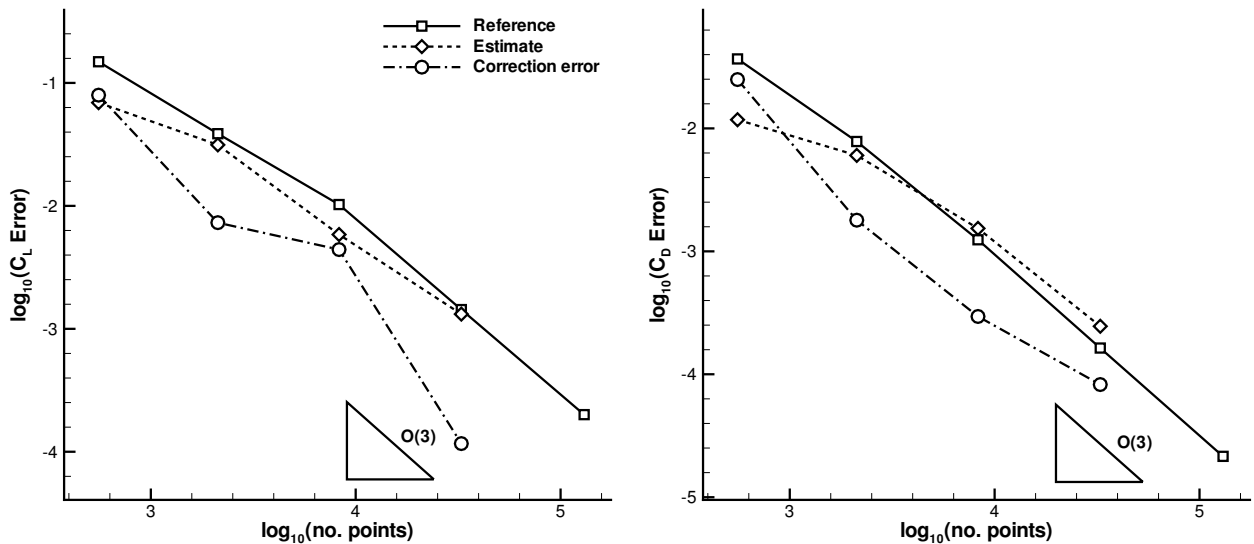
Figure 2: Convergence of lift and drag error with global mesh refinement for the subsonic turbulent RAE-2822. Shown are: an approximation to the true error based on Richardson extrapolated values (squares), the dissipation-based error estimate (diamonds), and the error in the value corrected with the estimate (circles).

Grid 4, with only 2000 points and $y^+ \simeq 10$, indicating very poor boundary-layer resolution. This provides an indication that mesh convergence is already sufficiently advanced by Grid 4 to make linearized methods useful, and gives hope that similar accuracy may be achieved on similarly coarse grids for more complex flow fields.

The detailed reproduction of individual "wiggles" in the error on Grid 2 is not fully understood, but is likely to be related to the use of the exact linearization of the spatial discretization in the ETE, which thereby incorporates all particulars and idiosyncrasies of the flow solver.

4.2 Application of Goal-Oriented Adaptation

4.2.1 Supersonic Aerofoil: NACA0012

The goal-oriented error indicator of (11) is briefly examined for a case which highlights the manner in which the adjoint solution captures the information transport properties of the flow. Consider an inviscid supersonic NACA0012 aerofoil with $M_\infty = 1.5$ and $\alpha = 1.0$, for which contours of pressure are shown in Figure 4. The flow is supersonic everywhere expect for a small region around the stagnation point; as a result information transport is to a large extent unidirectional and errors produced downstream of the aerofoil do not influence lift or drag. This behaviour is captured by the adjoint solution (also shown), which identifies the region upstream of the leading edge, and those characteristics which intersect with the trailing edge as having largest influence on the drag. The two terms of the indicator (16) are also plotted in Figure 4, where the relative influence and regional activation of the two dissipation terms — $k^{(2)}$ active near the shock, and $k^{(4)}$ partly switched off there — as well as the effect of the adjoint solution are visible. In front of the shock the solution is uniform, residuals are small, and hence the indicators are small despite the large adjoint solution there. The general irregularity of the indicator, which is partly due to its necessarily high sensitivity to the grid, demands that a small amount of smoothing is used. Here and in the following, two Laplacian smoothing passes with a coefficient of 0.5 are applied.

To quantify the effectiveness of the adjoint error indicator and estimator we consider goal-oriented adaptation of this case with respect to C_L and C_D. We proceed as follows: on the initial mesh a flow solution is computed, followed by an adjoint solution for J, based on which the error indicator and estimator are evaluated. The mesh is refined, whereby a fixed percentage of new points are added (in this case 40%), and a new flow solution is computed, etc. All components of this chain are parallelized and no stopping criterion is used, rather the calculation halts when the available computing resources are exhausted. The reference solution is obtained from an initial coarse mesh of 11×10^3 points, which is uniformly refined 5 times resulting in a mesh of about 11×10^6 points.

For the purposes of comparison a feature-based adaptation indicator is considered. The simple idea is that large errors are made locally where solution gradients are large with respect to the cell spacing. For some flow variable ϕ the indicator on a mesh face Γ_{ij} is [34]:

$$\xi_{ij}^{\mathrm{FB}} = \sum_\phi \omega_\phi h^q |\phi_j - \phi_i|, \tag{19}$$

where $q \geq 0$ adjusts the rate at which the indicator approaches zero as the mesh is refined, and ω_ϕ are constant flow variable weights. In the following $q = 0$ and the variables total pressure and total enthalpy are used with equal weighting.

The mesh convergence for C_L and C_D for the various methods is displayed in Figure 5 where all errors are calculated with respect to the reference solution. For the error indicator results the error estimate (18) and the therewith corrected coefficient values are also plotted. The uniformly refined meshes converge cleanly
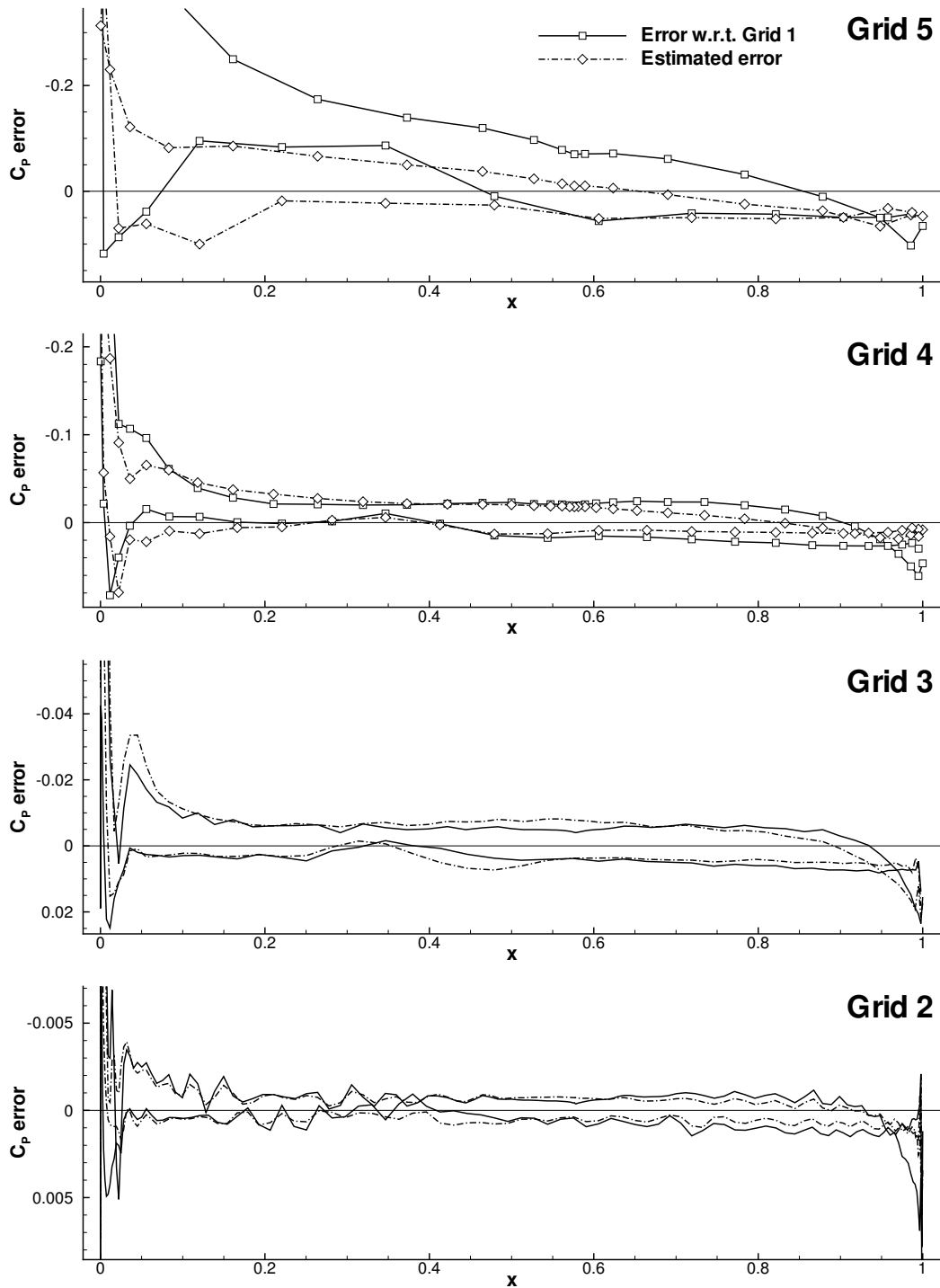
Figure 3: Error in surface pressure coefficients for th 4 coarse grids, calculated with respect to the finest (Grid 1) solution (solid lines), and estimated with the error transport equation using the dissipation residual (dashed lines).

Efficient *A Posteriori* Error Estimation for Finite Volume Methods
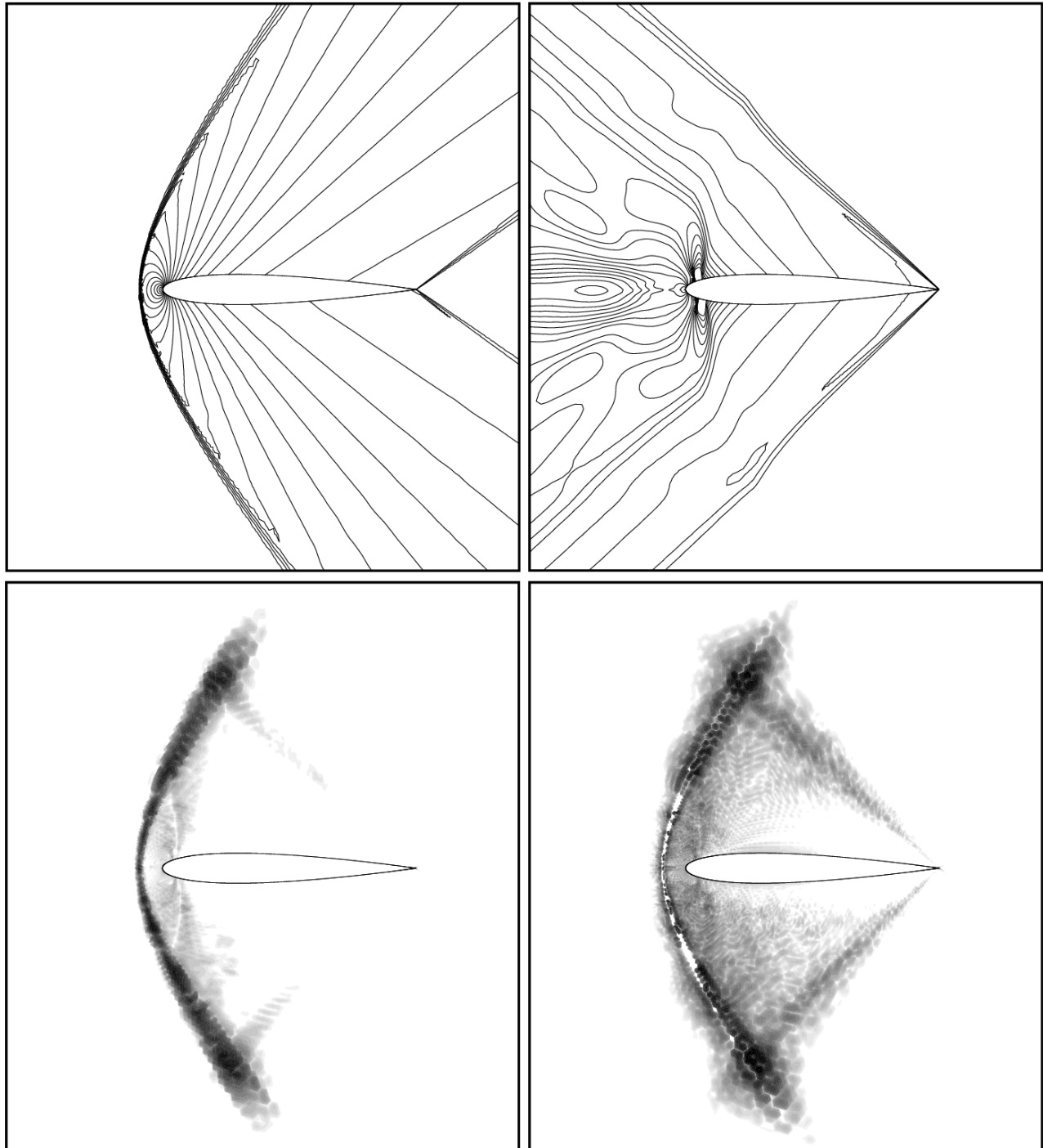
Figure 4: Error indicator contours for supersonic NACA0012 drag: pressure (top left), first adjoint variable (top right), $k^{(2)}$, $k^{(4)}$ sensitivity (bottom left, right respectively). The two sensor plots use the same (logarithmic) scale, where dark regions represent large indicator values.
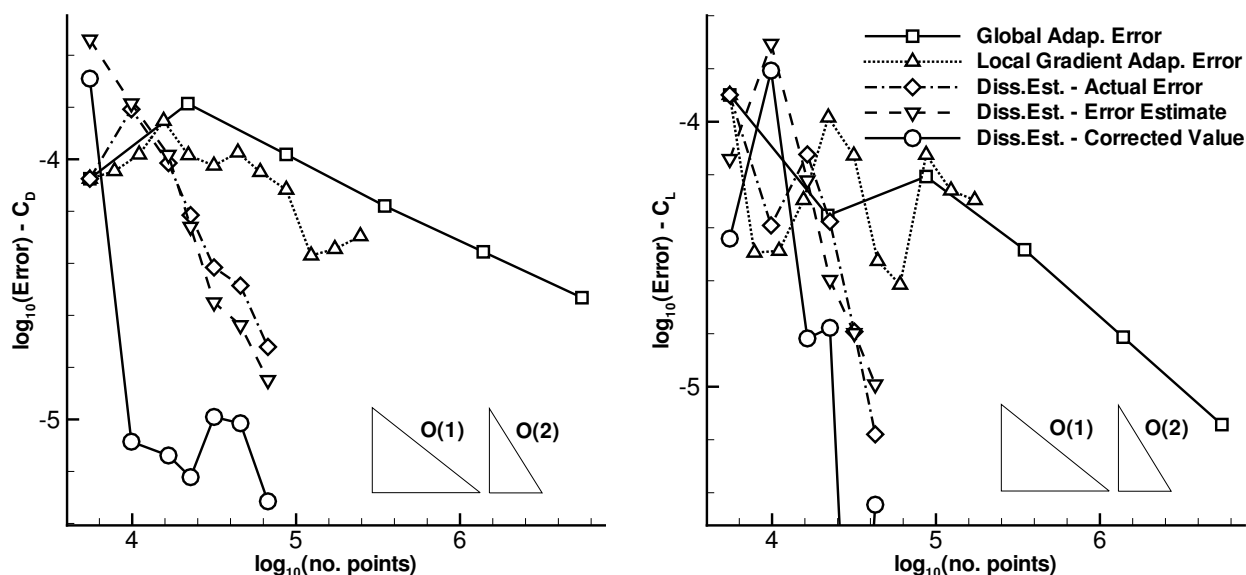
Figure 5: Convergence of C_D (left) and C_L (right) errors for global, local-gradient and dissipation-error refinement, the supersonic NACA0012 case. Error estimator and corrected error are shown for the dissipation-based indicator.

after initial non-linearities between the solutions on the first three meshes. The low order of convergence is a consequence of solution discontinuities.

Immediately evident is that the feature-based indicator converges poorly and irregularly, performing not much better than uniform refinement for C_D, and actually worse for C_L. For other test cases apparent convergence to incorrect solutions has even been observed. The poor suitability of standard feature-based indicators for strongly hyperbolic problems is well known, but these findings emphasize the pressing need for a cheap and reliable alternative.

The dissipation error indicator on the other hand, achieves the accuracy of the finest uniformly refined grid within 7 adaptation iterations, and with a factor of 100 less mesh points. Especially interesting is that the level of error achieved after each adaptation iteration corresponds roughly to the error in the corresponding uniform grid, suggesting that on each step the indicator is refining the mesh everywhere where a significant reduction in the error is to be made. The estimated error corresponds very well to the actual error for almost all points, and moderately well in the remaining two points. As a consequence the force coefficients corrected with the error estimate are on the whole significantly more accurate than the original force coefficients.

The meshes resulting from repeated local gradient based adaptation, and error indicator adaptation on C_L are shown in Figure 6, whereby the two grids have approximately the same number of points. The former mesh appears less dense because of the large numbers of points expended in the small region of the shock, and points far from the aerofoil, outside the frame of the figure. The error indicator mesh highlights the importance of the leading edge, the characteristics intersecting the trailing edge, and that part of the shock in a position to influence the surface pressure. Note that although the shock is well resolved it was not refined at *every* adaptation iteration as was the case with the standard indicator, which has over-resolved the shock at the expense of other important flow regions.
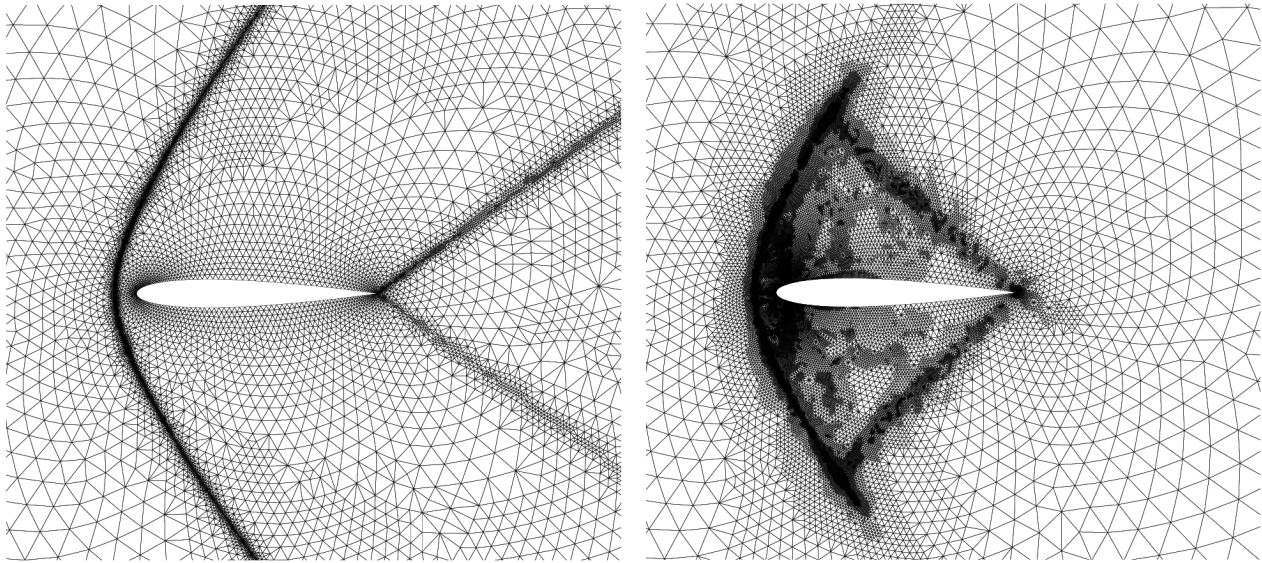
Figure 6: Meshes for the supersonic case obtained using adaptation with respect to local solution gradients (left), and the dissipation-based error indicator (right). The two grids have a similar number of points.

4.2.2   Transonic wing: ONERA M6

In three-dimensions we consider — what has become a standard 3d transonic test case — the ONERA M6 wing at an angle-of-attack of $\alpha = 3.06$, and far-field Mach number of $M_\infty = 0.84$. Surface pressure contours are shown in Figure 7 where the familiar lambda shock structure is visible.

Convergence results are given in Figure 8. Horizontal lines mark typical engineering accuracy bounds of ± 5 drag counts, and ± 0.5 lift counts. Feature-based adaptation can be seen to perform poorly, and the error indicator significantly better, however particularly striking is that the error estimator corrected force coefficient values all lie within the given accuracy bounds, even on the initial grid — in fact the estimator is most accurate on the initial grid. This may be a consequence of the error that is estimated, being the same as the error that is reduced by the adaptation. As the adaptation progresses that part of the error not due to dissipation will eventually dominate. Cuts through the grids obtained with the two adaptation methods are given in Figure 9 where the relative irregularity of the grid based on the error indicator is evident. This suggests the need for more sophisticated smoothing than that applied at present, as irregular grids have a strong influence on the stability and accuracy of finite volume methods.

5.0   CONCLUSIONS AND FURTHER WORK

It has been demonstrated that error estimation techniques may be applied efficiently and effectively in a finite volume framework by using a discrete linearization of the flow solver and a local estimate of residual error based on explicitly added artificial dissipation. This technique relies on the dominance of this dissipation over the remaining part of the discretization error. This dominance has been previously demonstrated to be the case for the unstructured finite volume method presently considered, and for the level of accuracy in which engineers are principally interested [18].

The resulting estimator has been shown to accurately estimate the error in force coefficients and entire
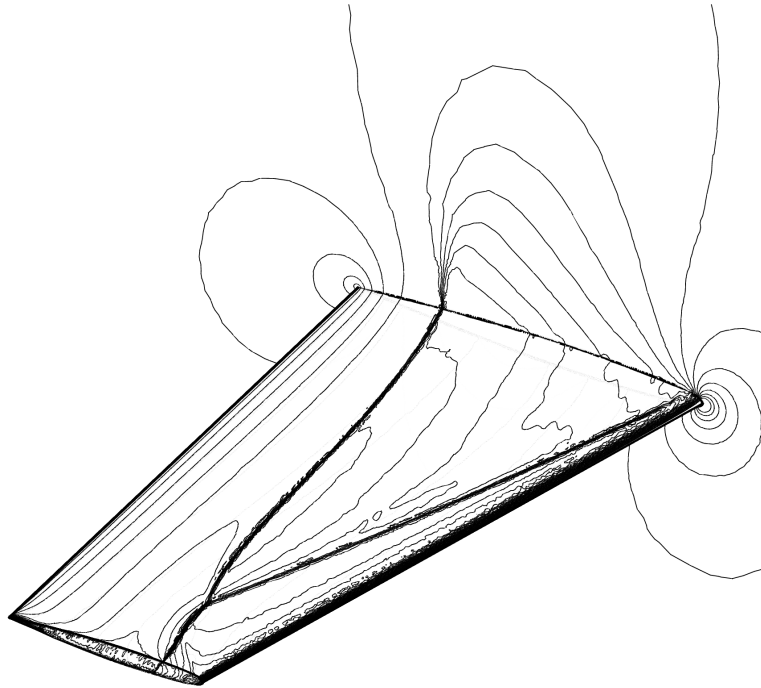
Figure 7: Transonic ONERA M6 wing test-case with lambda shock structure.
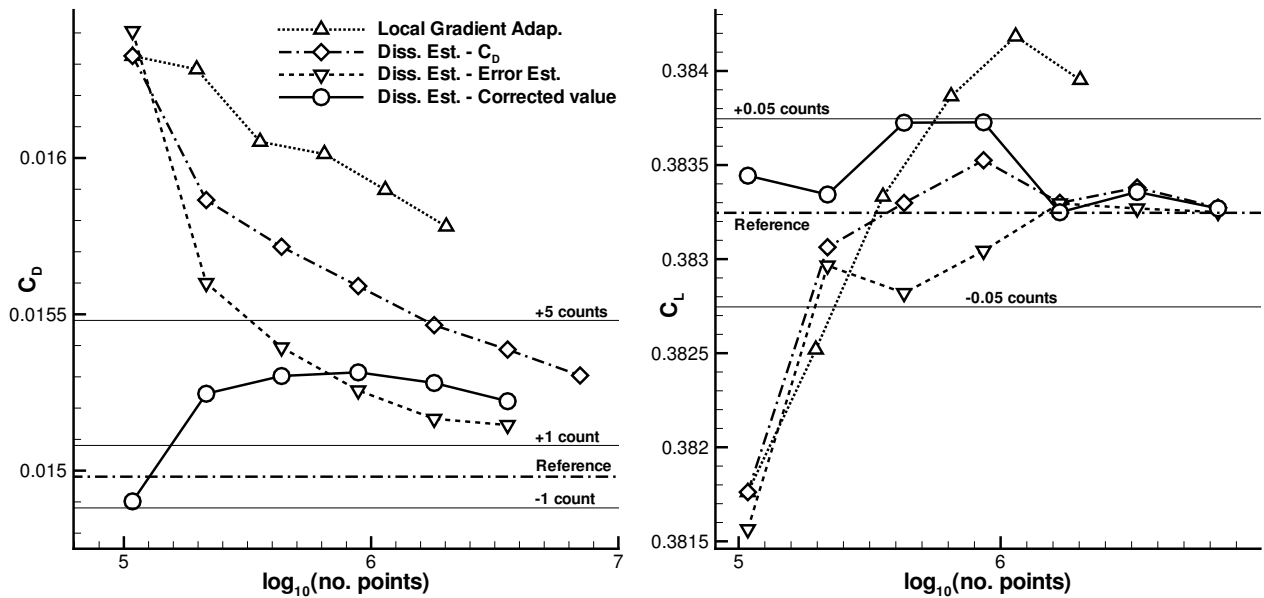
Figure 8: Convergence of C_D (left) and C_L (right) for local-gradient and dissipation-error refinement for the ONERA M6 wing. Error estimator and corrected solution are also plotted.
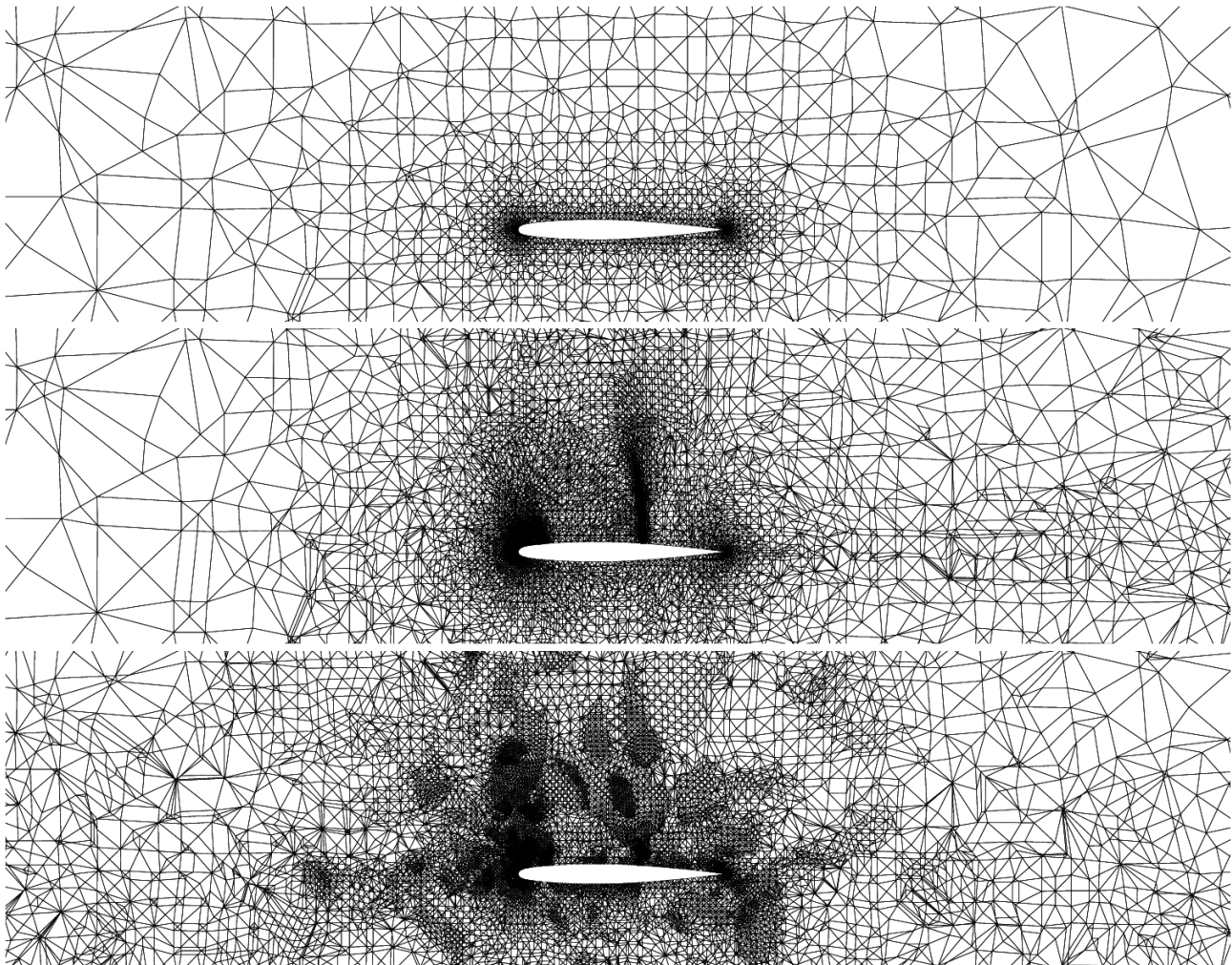
Figure 9: ONERA M6 initial, local-gradient, and error indicator (drag) adapted grids cut at $y = 6$. The two adapted grids have a similar number of nodes.

pressure distributions for 2d Navier-Stokes calculations, while the corresponding adjoint formulation has been seen to provide a mesh adaptation indicator which considerably out-performs local-gradient based indicators.

Future activities should include comparison of the dissipation-based estimator with estimators based on residuals obtained from globally refined grids. Though it is clear from the results presented that the dissipation-based estimator is effective, it is difficult to judge how much more accuracy in the estimator may be obtained by using an improved residual. In a similar vein the current approach should be implemented in other finite volume solvers to ensure that the results do not depend on some special feature of the particular solver used.

Finally: goal-oriented adaptation may be applied to problems with n functionals of interest J_i without solving n separate adjoint problems. If the sign of the error e_i in each J_i is known, say $s_i \in \{-1, 1\}$, then a composite functional may be constructed as

$$\bar{J} := \sum_i s_i J_i,$$

in which the component errors do not cancel. The single adjoint problem corresponding to $\bar{J}$ then gives an error indicator for $\sum_i |e_i|$. All s_i may be approximated with a single solution of the error transport equation. This approach will be examined in future work.

Acknowledgments

References

[1] Gerhold, T., Galle, M., Friedrich, O., and Evans, J., "Calculation of Complex 3D Configurations Employing the DLR TAU-Code," *AIAA Paper Series, AIAA-1997-0167*, 1997.

[2] Dwight, R., *Efficiency Improvements of RANS-Based Analysis and Optimization using Implicit and Adjoint Methods on Unstructured Grids*, Ph.D. thesis, School of Mathematics, University of Manchester, 2006.

[3] Edwards, J. and Chandra, S., "Comparison of Eddy-Viscosity Transport Turbulence Models for Three-Dimensional Shock-Seperated Flowfields," *AIAA Journal*, Vol. 34, No. 4, 1996, pp. 1–16.

[4] Jameson, A., Schmidt, W., and Turkel, E., "Numerical Solutions of the Euler Equations by Finite Volume Methods Using Runge-Kutta Time-Stepping Schemes," *AIAA Paper Series, AIAA-1981-1259*, 1981.

[5] Cavallo, P. and Sinha, N., "An Error Transport Equation with Practical Applications," *AIAA Paper Series, Paper 2007-4092*, AIAA, 2007.

[6] Giles, M. and Pierce, N., "Analytic adjoint solutions for the quasi-one-dimensional Euler equations," *Journal of Fluid Mechanics*, Vol. 426, 2001, pp. 327–345.

[7] Barth, T., "A-Posteriori Error Estimation and Mesh Adaptivity for Finite Volume and Finite Element Methods," *Springer series Lecture Notes in Computational Science and Engineering*, Vol. 41, 2004.

[8] Johnson, C., Rannacher, R., and Boman, M., "Numerics and hydrodynamics stability theory: Towards error control in CFD," *SIAM Journal of Numerical Analysis*, Vol. 32, 1995, pp. 1058–1079.

[9] Giles, M., Larson, M., Levenstam, M., and Süli, E., "Adaptive Error Control for Finite Element Approximations of the Lift and Drag Coefficients in Viscous Flow," Tech. Rep. NA-97/06, Comlab, Oxford University, 1997.

[10] Süli, E., "A posteriori error analysis and adaptivity for finite element approximations of hyperbolic problems," *An Introduction to Recent Developments in Theory and Numerics for Conservation Laws, Volume 5 of Lecture Notes in Compuational Science and Engineering*, edited by Kröner, Ohlberger, and Rohde, Springer, Heidelberg, 1998, pp. 122–194.

[11] Prudhomme, S. and Oden, J., "On goal-oriented error estimation for elliptic problems: application to the control of pointwise errors," *Comp. Meth. Appl. Mech. and Eng.*, 1999, pp. 313–331.

[12] Hartmann, R. and Houston, P., "Adaptive discontinuous Galerkin methods for the compressible Euler equations," *Journal of Computational Physics*, Vol. 182, No. 2, 2002, pp. 508–532.

[13] Venditti, D. and Darmofal, D., "Anisotropic grid adaptation for functional outputs: Application to two-dimensional viscous flows," *Journal of Computational Physics*, Vol. 187, 2003, pp. 22–46.

[14] Pierce, N. and Giles, M., "Adjoint and Defect Error Bounding and Correction for Functional Estimates," *Journal of Computational Physics*, Vol. 200, 2004, pp. 769–794.

[15] Jones, W., Nielsen, E., and Park, M., "Validation of 3D Adjoint Based Error Estimation and Mesh Adaptation for Sonic Boom Prediction," *44th AIAA Aerospace Sciences Meeting and Exhibit, Reno, Nevada. Paper AIAA-2006-1150*, 2006.

[16] Nemec, M. and Aftosmis, M., "Adjoint Error Estimation and Adaptive Refinement for Embedded-Boundary Cartesian Meshes," *18th AIAA CFD Conference, Miami. Paper AIAA-2007-4187*, 2007.

[17] Dwight, R., "Goal-Oriented Mesh Adaptation using a Dissipation-Based Error Indicator," *International Journal of Numerical Methods in Fluids*, 2007, DOI: 10.1002/fld.1582.

[18] Dwight, R., "A Posteriori Estimation of Error due to Dissipation in Finite Volume Schemes and Application to Mesh Adaptation," *18th AIAA CFD Conference, Miami. Paper AIAA-2007-4093*, 2007.

[19] Pironneau, O., "On Optimum design in fluid mechanics," *Journal of Fluid Mechanics*, Vol. 64, No. 2, 1974, pp. 97–110.

[20] Jameson, A., "Aerodynamic design via control theory," *Journal of Scientific Computing*, Vol. 3, No. 3, 1988, pp. 233–260.

[21] Bristow, D. and Hawk, J., "Subsonic Panel Method for Designing Wing Surface from Pressure Distribution," Tech. Rep. CR 3713, NASA, 1983.

[22] Taylor III, A., Korivi, V., and Hou, G., "Sensitivity analysis applied to the Euler equations: A feasibility study with Emphasis on Variation of Geometric Shape," *AIAA Paper Series, Paper 91-0173*, 1991.

[23] Jameson, A., Martinelli, L., and Pierce, N., "Optimum aerodynamic design using the Navier-Stokes equations," *Theoretical and Computational Fluid Dynamics*, Vol. 10, No. 1, 1998, pp. 213–237.

[24] Jameson, A., Alonso, J., Reuther, J., Martinelli, L., and Vassberg, J., "Aerodynamic Shape Optimization Techniques based on Control Theory," *AIAA Paper Series, Paper 98-2538*, 1998.

[25] Newman III, J., Taylor III, A., Barnwell, A., Newman, P., and Hou, G., "Overview of Sensitivity Analysis and Shape Optimization for Complex Aerodynamic Configurations," *Journal of Aircraft*, Vol. 36, No. 1, 1999, pp. 97–116.

[26] Nadarajah, S. and Jameson, A., "A comparison of the continuous and discrete adjoint approach to automatic aerodynamic optimization," *AIAA Paper Series, Paper 2000-667*, 2000.

[27] Nemec, M. and Zingg, D., "A Newton-Krylov Algorithm for Aerodynamic Design Using the Navier-Stokes Equations," *AIAA Journal*, Vol. 40, No. 6, 2002, pp. 1146–1154.

[28] Dwight, R., Brezillon, J., and Vollmer, D., "Efficient Algorithms for Solution of the Adjoint Compressible Navier-Stokes Equations with Applications," *Proceedings of the ONERA-DLR Aerospace Symposium (ODAS), Toulouse*, 2006.

[29] Dwight, R. and Brezillon, J., "Effect of Approximations of the Discrete Adjoint on Gradient-Based Optimization," *AIAA Journal*, Vol. 44, No. 12, December 2006, pp. 3022–3071.

[30] Giles, M., "On the Iterative Solution of the Adjoint Equations," *Automatic Differentiation: From Simulation to Optimization*, 2001, pp. 145–152.

[31] Saad, Y. and Schultz, M. H., "GMRES: A generalized minimum residual algorithm for solving non-symmetric linear systems," *SIAM Journal of Scientific and Statistical Computing*, Vol. 7, No. 3, 1988, pp. 856–859.

[32] Campobasso, M. and Giles, M., "Stabilization of a linear flow solver for turbomachinery aeroelasticity by means of the recursive projection method," *AIAA Journal*, Vol. 42, No. 9, 2004, pp. 1765–1774.

[33] Cook, P., McDonald, M., and Firmin, M., *Aerofoil RAE 2822 — Pressure Distributions and Boundary Layer and Wake Measurements*, chap. 6, No. 138 in AGARD–AR, AGARD — Advisory Group for Aerospace Research & Development, Neuilly-sur-Seine, France, 1979.

[34] Alrutz, T. and Rütten, M., "Investigation of Vortex Breakdown over a Pitching Delta Wing applying the DLR TAU-Code with Full, Automatic Grid Adaptation," Paper 5162, AIAA, 2005.

Efficient *A Posteriori* Error Estimation for Finite Volume Methods

Paper No. 46

Discusser's Name: P. Raj

Question: Have you looked at the sensitivity of solutions to numerical schemes at the boundary?

Authors' Reply: No, but this is currently and in future an area of intense investigation, especially with regard to the dissipation operator at the boundary.

Discusser's Name: Bil Kleb

Question: How do you specify the mesh adaptation schedule for both your feature-driven and adjoint-driven adaptation and is there a method (besides "ad hoc") for determining it?

Authors' Reply: In both cases the number of new points is specified as a percentage of existing points. For example the adaptation indicator may be distributed in [0,1], and we iterate on some threshold value c (using repeated bisection) until the required number of points is approximately achieved. Within each step of the iteration, no mesh modification is made, only mesh elements are marked.

Discusser's Name: J. Benek

Question: With explicit dissipation the formulation is straight forward. How will it work for methods where dissipation is implicit in flux formulation?

Authors' Reply: Every consistent flux may be written as a central difference plus a dissipation term. In order to extend the method, simply add a fictive parameter , multiplying the dissipation term with nominal value 1, and examine the influence of perturbations of this parameter. Because in general fluxes have 2nd order accurate in space dissipation terms, this should work better than for the central scheme (with 3rd order dissipation)